A&A 397, 227–236 (2003)
DOI: 10.1051/0004-6361:20021480

Astronomy & Astrophysics

Near and Mid-infrared images of the massive star forming complex G9.62+0.19⋆

P. Persi[1], M. Tapia[2,6], M. Roth[3], A. R. Marenzi[1], L. Testi[4], and L. Vanzi[5]

[1] Istituto Astrofisica Spaziale e Fisica Cosmica, CNR, Via del Fosso del Cavaliere, 00133, Roma, Italy
e-mail: persi@rm.iasf.cnr.it
[2] Instituto de Astronomía, UNAM, Apartado Postal 877, Ensenada, Baja California, CP 22833, Mexico
[3] Las Campanas Observatory, Carnegie Institution of Washington, Casilla 601, La Serena, Chile
[4] Osservatorio Astrofisico di Arcetri, Largo E. Fermi 5, 50125 Firenze, Italy
[5] European Southern Observatory, Alonso de Cordoba 3107, Santiago, Chile
[6] Harvard-Smithsonian Center for Astrophysics, 60 Garden St, Cambridge, MA 02138, USA

Received 26 April 2002 / Accepted 8 October 2002

Abstract. A near- and mid-infrared study of the star formation complex G9.62+0.19 is presented. It includes photometrically calibrated images through wide-band *JHK* and narrow-band Brγ, H_2 and 12.5 μm filters. These were taken at Las Campanas, La Silla and OAN-San Pedro Mártir. We found evidence of two embedded young clusters of O-B5 stars associated with the radio components B and C, one compact and one ultracompact HII region. The data suggest the presence of a third, more dispersed cluster of more luminous infrared stars at the southern edge of the cloud complex. A large fraction of the star members of each cluster exhibit significant infrared excess. We confirm the detection of a very red near- and mid-infrared source immersed in the molecular hot core (component F). An H_2 shocked gas knot, probably an obscured Herbig-Haro object, was found associated to the blue-shifted lobe of the high-velocity molecular outflow in this core. The properties of the individual sources are discussed in detail.

Key words. stars: formation – infrared: stars

1. Introduction

Located at a distance of 5.7 kpc (Hofner et al. 1994), G9.62+0.19 is a massive star-forming region characterized by the presence of a number of ultracompact (UC) HII regions (named D-I by Garay et al. 1993 and Testi et al. 2000), H_2O, OH, CH_3OH (methanol) and NH_3(4,4) (ammonia) maser sources in a molecular core which was mapped in the $NH_4C^{18}O$ (1-0) and CH_3CN (6-5) lines by Cesaroni et al. (1994) and Hofner et al. (1996), respectively. Inside this core, between the UC HIIs D and E, a so-called hot molecular core (HMC) source (component F) is located. This object is believed to be a precursor of an UC HII region (Cesaroni et al. 1994) and is thought to be responsible for driving a molecular outflow (Hofner et al. 2001). The presence of an embedded young massive star within the HMC is supported by the detection of a faint radio continuum emission at the position of the core (Testi et al. 2000) and of a 2.2 μm source probably associated with it (Testi et al. 1998).

Just outside the molecular core, to the W and NW, three compact, more evolved, HII regions (A, B and C) are present. Component A is the largest (32″) and westernmost. Its extension and low surface temperature indicate that it is the oldest in the complex. Component B, located close to the edge of the core, is a smaller (15″) cometary-shaped HII region (Kurtz et al. 1994) which is also detected in the near-infrared (Testi et al. 1998). Component C, some 20″ further north, is classified as an ultracompact HII region (Garay et al. 1993).

Previous studies indicated that several very young massive stellar objects at different evolutionary stages are present in G9.62+0.19. To explain this, a simple evolutionary model has been proposed by Testi et al. (1998) in which the observed properties of the individual components of the complex fit into a well established evolutionary sequence.

This paper presents an infrared study of G9.62+0.19 based on sub-arcsec-resolution near and mid-IR images. In Sect. 2 the observations are described, while in Sect. 3 an analysis of

Send offprint requests to: P. Persi,
e-mail: persi@rm.iasf.cnr.it

⋆ Partly based on observations collected at the European Southern Observatory, La Silla, at the Las Campanas Observatory, Chile and at the Observatorio Astronómico Nacional, San Pedro Mártir, Mexico.

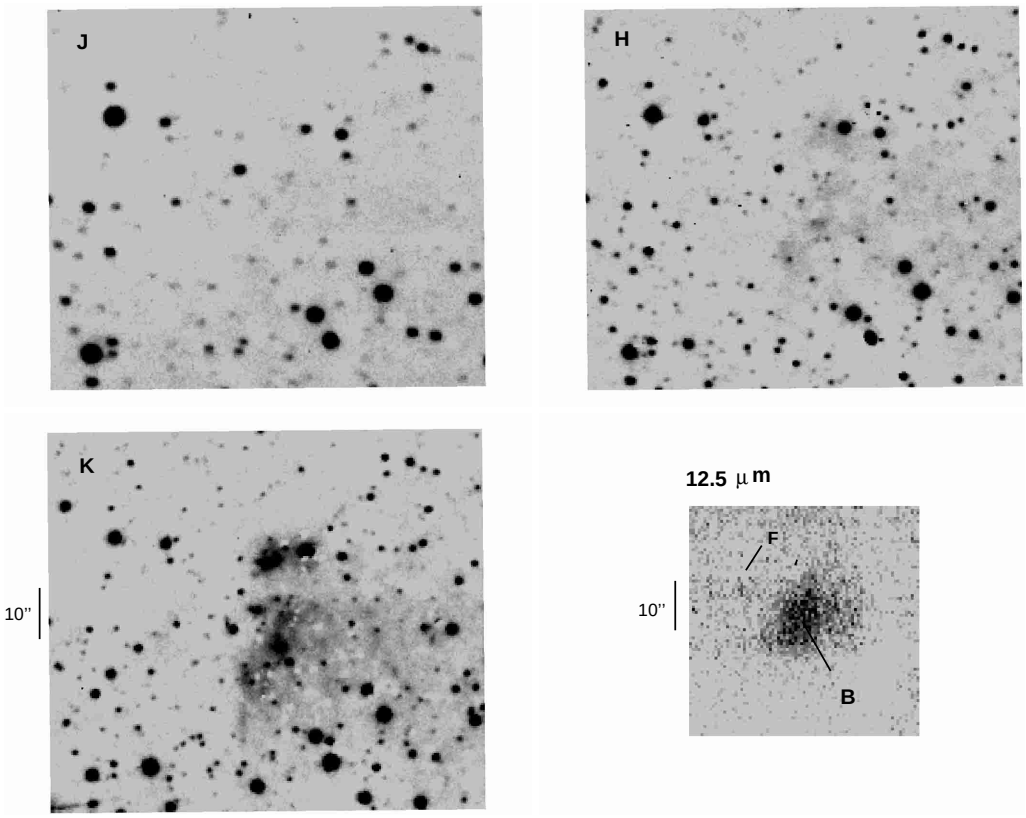

Fig. 1. Campanas J, H, K and SPM 12.5 μm images of G9.62+0.19. North is the top and east to the left.

the young stellar population based on the JHK images is presented. Finally in Sect. 4 we discuss the infrared sources associated with the several compact and ultra-compact HII regions.

2. Observations

2.1. Near-infrared images

Two sets of J, H and K-band images were taken. One with the NICMOS3 array camera attached to the 2.5 m Dupont telescope of Las Campanas Observatory (Chile) on 21 May 1997. In each band, five partially overlapping frames were taken, covering a total area of $178'' \times 178''$ centered approximately at the HMC position. The image scale was 0.35″/pix, and the mean PSF was approximately 0.8″ ($FWHM$). The integration times were 120 s in K, 300 s in H and 380 s in J. The images were photometrically calibrated observing the standard stars in use at Las Campanas at similar airmass. Stellar photometry was derived using the DAOPHOT (Stetson 1987) package within the IRAF environment with an aperture of 2″. In the central overlapping area of size $89'' \times 89''$ where the signal to noise ratio is higher, 292 sources were detected in K, 227 in H and 136 in J with sensitivity limits (3σ) of 17.5 at K, 18,8 at H and 19.8 at J. The average photometric errors in all colors are 0.06 for sources at least 1.5 mag brighter than these limits and up to 0.2 for the faintest sources. In order to check our calibration we compared, for the sources in common, DENIS (Epchtein et al. 1999) photometry with ours. These agree within the quoted errors. The JHK images together with the 12.5 μm image described in Sect. 2.2 are presented in Fig. 1. The table with positions and photometry of all measured sources is available electronically from the authors upon request.

A more extended region was also observed using the ESO-NTT 3.6 m telescope and the SofI near-infrared multi-mode instrument in August and September 2000. Images were obtained through J, H, and K_s broad-band filters and through three narrow-band filters centered on the H_2(1–0) S(1) and Brγ lines at 2.122 μm and 2.165 μm, respectively. The continuum level was defined by obtaining an image at 2.195 μm. Following standard data reduction, the narrow-band images were aligned, PSF-matched and continuum subtracted using the ISIS package (Alard 2000). The average seeing was ∼0.6″ for the JHK_s and the integration time was 15 min for each filter. Although the images were very deep ($K_s < 19.5$, $H < 20.5$ and $J < 21.5$), the conditions did not allow good quality photometric calibrations. For this reason, the Las Campanas photometry was chosen for the present analysis. During the narrow band observations, the average seeing was ∼1.5″. The integration times were 20 min for Brγ and 40 min for H_2.

Accurate astrometry was performed using the position of a set of 20 bright near-IR stars from the DENIS survey in common with our images. The measured standard deviation of our positions (relative to DENIS) was 0.″5 in both right ascension and declination. Allowing for the quoted DENIS position errors, we estimate the accuracy of our coordinates to be better than 1″.

SofI broad-band and continuum-subtracted H_2 images of the area containing the UC HII regions D, E, C and the HMC (F) are shown in Fig. 2. Molecular hydrogen emission

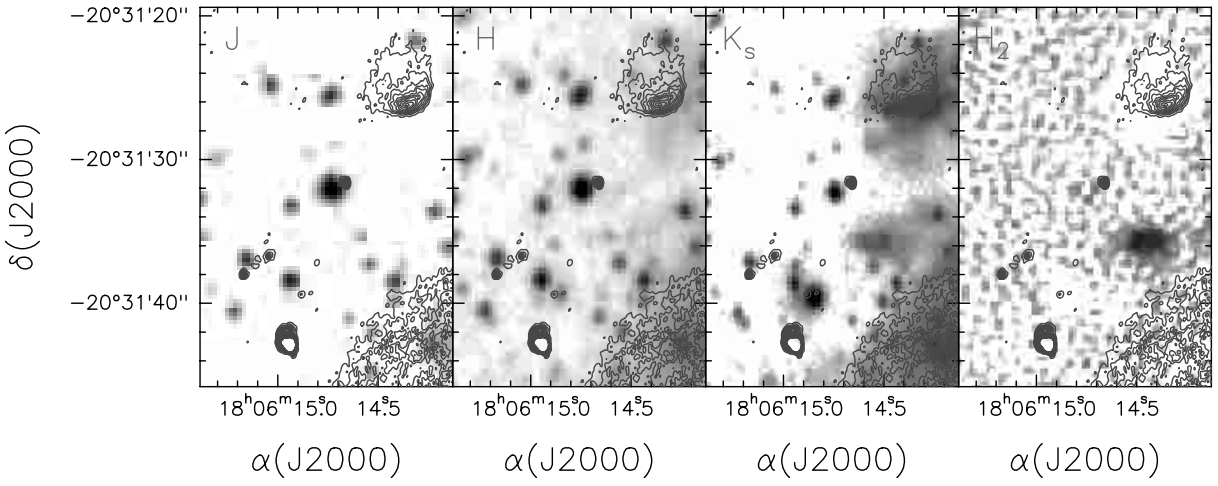

Fig. 2. NTT J, H, K_s, and continuum-subtracted H_2 images of the area containing the UC HII regions D, E, C and the HMC (F). In each panel the contour plot of the 3.6 cm radio continuum emission from Testi et al. (2000) is overlaid.

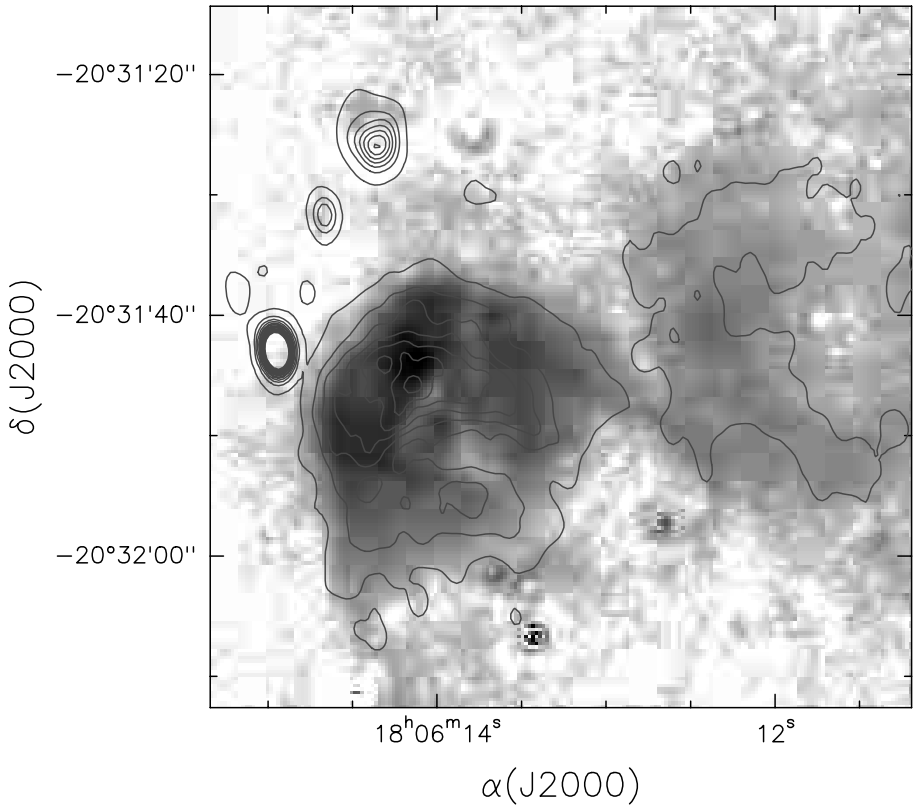

Fig. 3. Continuum-subtracted Brγ SofI image of the G9.62+0.19 region. The contour plot shows the 2 cm radio continuum emission from Testi et al. (2000).

is detected only in the field shown. Figure 3 shows the continuum-subtracted Brγ image and a comparison with the radio-continuum emission (Testi et al. 2000).

2.2. Mid-IR image

The image at 12.5 μm ($\Delta\lambda$ = 1.2 μm) centered on the HMC was taken on 13 September 2000, with CID, a mid infrared camera (Salas et al. 2002) attached to the 2.12 m telescope of the Observatorio Astronómico Nacional at San Pedro Mártir, B.C, Mexico. CID is equipped with a Rockwell 128×128 pixel Si:As blocked impurity band (BIB) detector array. The field of view of the array is 70″ × 70″ with an effective scale of 0.55″/pix. Sky and telescope emission is removed using the standard chop-nod technique. The image was calibrated using the mid-infrared San Pedro Mártir standard star system (Salas et al. 2002). With our adopted on-source integration time we derived a 1-σ noise of 13.6 mJy/pix.

The mid-infrared image is characterized by the presence of diffuse emission extending NW-SE (Fig. 1), and a faint

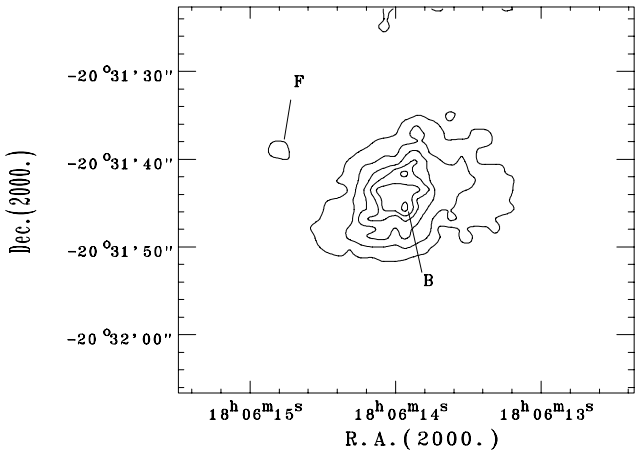

Fig. 4. Contour map at 12.5 μm of G9.62+0.19 where the radio HII region B and the HMC F are labelled.

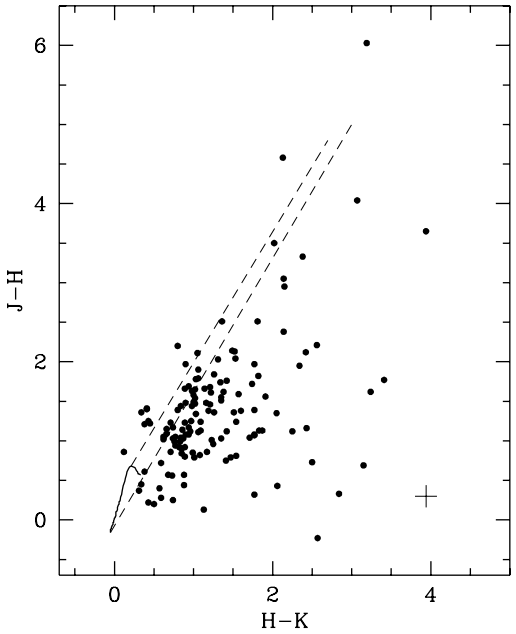

Fig. 5. $J-H$ vs. $H-K$ diagram of 136 sources detected in G9.62+0.19. The continuous line marks the loci of the main sequence stars (MS) from Koornneef (1983). The two parallel dashed lines represent the standard reddening vectors for late and early-type stars. The cross indicates the mean photometric error.

point-like source. We derived a flux density at 12.5 μm of 24.3 ± 1.79 Jy with an aperture of 10″ for the extended source. This value is in agreement with the MSX flux of 31 ± 1.8 Jy in band C (12.1 μm; Egan et al. 1999) taken with a larger aperture. As determined by the ISO SW spectrum (Peeters et al. 2002) of this source, the detected flux in these pass-bands is dominated by a strong [NeII] (12.81 μm) line emission with a weak underlying continuum.

For the point-like source we measured a flux of 0.5 ± 0.3 Jy with a 3″ aperture. The astrometric calibration of this image is difficult due to the lack of nearby reference objects. Its position was, nevertheless, determined by measuring the separation between the faint point-like object and the centroid of the mid-IR extended emission from component B as given by the MSX satellite catalogue (Egan et al. 1999: α_{2000} = $18^h06^m13.9^s$; δ_{2000} = −20°31′45″). This offset position is $+0.74^s$ in right ascension and +5.3″ in declination with a 1–2″ accuracy due to the uncertainty in determining the centroid of the extended source on our images. The result confirms that the new 12.5 μm unresolved source is the mid-IR counterpart of the radio HMC (see Fig. 4).

3. Discussion

3.1. The young stellar population

The $J-H$ vs. $H-K$ diagram of the 136 sources detected in all three filters is illustrated in Fig. 5. Considering the mean photometric errors illustrated by a cross in Fig. 5, we found that the location of most sources is consistent with normal reddened stars with values of A_V between 10 and 25, depending on the spectral type. Nevertheless, 20% of the sources were found to show significant infrared excess. The positions and photometry of these 27 sources are listed in Table 1.

In addition, nearly a hundred sources measured in the H and K bands were fainter than our detection limit in J due to their very red colors. In order to determine the nature of these sources, we analyzed the K vs. $H-K$ plot of all sources (left panel of Fig. 6). Distinction was made between sources measured in JHK with and without significant near-infrared excess and those measured only in HK. There seems to be a clear correlation pattern between the spatial position of the stars with their position in the K vs. $H-K$ diagram. To illustrate this, the right panel of Fig. 6 shows the position in the sky of all sources. Different colors were used for stars with infrared excesses immersed in the extended HII region G9.62+0.19B (red), in the UC HII region G9.62+0.19C (magenta) and for several luminous scattered stars (blue) with JHK colors characteristic of reddened ($A_V \simeq 6-15$) photospheres, though a few showed IR-excess (green). The last group is comprised of (mostly) very K-bright stars located to the south of G9.62+0.19B. Most of these are located on the upper part of the K vs. $H-K$ diagram implying that (at the distance of 5.7 kpc) they are O-B0 stars. Again, most of them show large infrared excess. The members of this surprising group of young massive stars are less reddened than those immersed in the radio HII regions and, although still with circumstellar dust envelopes, they seem to be more massive and less young than those closer to the hot molecular core.

We identify most of the other sources (in black) with foreground stars, although statistically we expect nearly all the sources with $H-K \geq 2$ to be young stellar objects also associated with G9.62+0.19.

The infrared morphology and structure of the complex is best seen in the "color-coded" JHK mosaic of our study area centered on G9.62+0.19 and covering 89 × 89 square arcsec shown in Fig. 7. It is striking that the fraction of very red objects, both diffuse and point-like, that have been discussed before is so large. The most extended and very red diffuse emission near the center of the image is associated with the HII region B and, as will be discussed in Sect. 3.2.1, is dominated by the Brγ line.

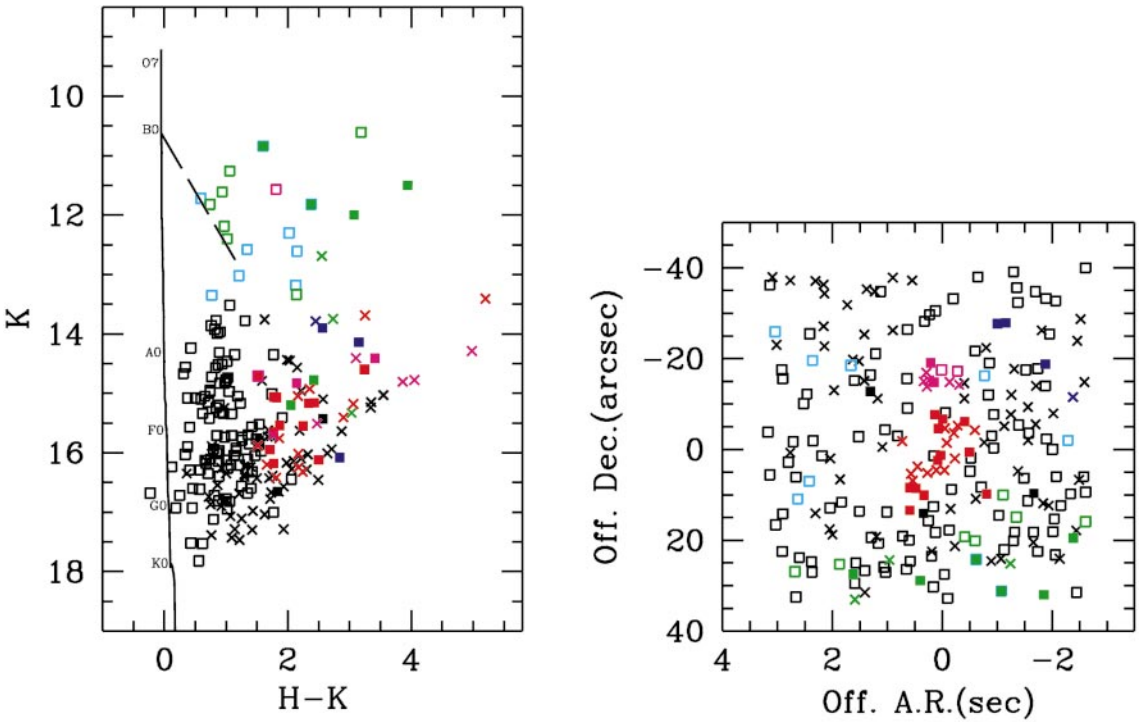

Fig. 6. *Left panel:* K vs. $H-K$ diagram of the sources found in G9.62+0.19. The continuous line is the loci of the main sequence stars at $d = 5.7$ kpc, while the dashed line is the reddening vector corresponding to $A_V = 20$. *Right panel:* Position of the same sources. The origin is at $\alpha_{2000} = 18^h06^m14.0^s$; $\delta_{2000} = -20°31'40''$. Filled squares are sources with significant JHK IR excess and open squares are sources without IR excesses from their JHK colors. Crosses are sources with HK colors but not detected in J. Different colors are used for sources located in certain regions. See Sect. 3.1.

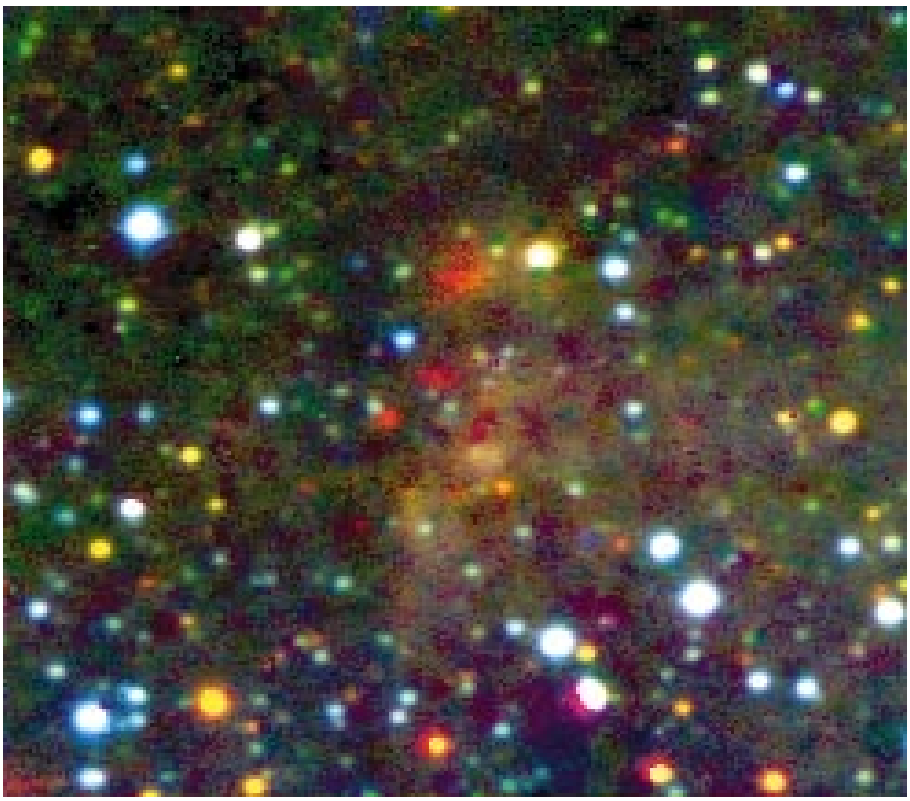

Fig. 7. Color-coded image of G9.62+0.19 made from J (blue), H (green), and K (red) mosaics covering $89'' \times 89''$. North is to the top, east to the left.

From the analysis of the color-color and color-magnitude plots (Figs. 5 and 6), we were able to identify at least 95 sources (27 with JHK excesses and 68 with $H-K>2$ and undetected in J) associated with the star forming region, most probably forming several clusters, some still deeply embedded in the cloud while at least another cluster is emerging out of it. This is also confirmed by the analysis of the observed K-magnitude distribution. In Fig. 8, we compare the K-magnitude distribution of the 95 sources identified as being associated with the cloud (dashed line) with that of sources classified as field stars (the rest; thick continuous line). Both histograms were normalized at bin $K=16.5$ by multiplying the number of IR-excess stars by 2.0 in order to show the differences in shape more clearly. For illustration, the distribution of (mostly field) stars counted from the 2MASS survey in a neighboring region outside the molecular cloud and normalized to the same area is also shown (thin continuous line). The latter has been extrapolated to fainter magnitudes and shifted horizontally in order to account for $A_K=2.6$, corresponding to $A_V=23$, the obscuration caused by the molecular cloud. It is clear that the distribution of the IR-excess stars differs significantly from that of the, mostly, field stars. There is a significant excess in the number of stars associated with G9.62+0.19 at $K<16$, with two or three peaks, the most conspicuous with K between 14.5 and 15.5, another with $K=13-14$ and also with $K=10.5-12.5$. From the analysis of Fig. 6, we associate the latter with a cluster of more massive (O-B0) stars, some still with circumstellar dust envelopes, with average extinction of $A_V\simeq 5-15$, implying that these have already dispersed a fraction of the dust and gas and whose UV radiation contribute to the ionization of the HII regions.

The less luminous IR-excess sources located within the boundaries of the radio HII regions G9.62+0.19B and G9.62+0.19C appear to form two clusters. The one associated with component B is more highly reddened with a mean $A_V=23$ with M_K and intrinsic $H-K$ colors consistent with spectral types B1 – B4. The stars associated with the more compact component C seem to be more luminous and still more deeply embedded, with a mean $A_V>25$.

With the present data, it is impossible to determine unambiguously further properties of the embedded clusters but, given the high number of massive stars with near-IR excess, it is very probable that star formation in this complex started less than 10^6 years ago.

The position of the 27 sources with IR-excess of Table 1 are marked as white crosses on the K-band image presented in Fig. 9. The position of the compact and ultracompact HIIs (B, C, D, E, open circles), of the hot molecular core (F black cross) and where the extended mid-IR source peaks (diamond, taken from the MSX catalogue) are also indicated in the figure. It is important to note that practically all the members of this very young embedded stellar population are located to the west and south-west of the methyl cyanid (CH_3CN) peak emission (Hofner et al. 1996) which probes the high density molecular gas. Clearly, this tells us that star formation began at the south and western edge of the molecular cloud and, as will be discussed later, is now active in the densest core to the NE.

3.2. Radio components outside the dense core

3.2.1. G9.62+0.19 B

The VLA maps at 1.3 cm (Cesaroni et al. 1994) and at 6 cm (Garay et al. 1993) show that this is a cometary-shaped HII region with an angular diameter of approximately 15–20″ and which is ionized by the UV radiation from at least one O6-O7.5 star. The sizes of the emission regions at 2.2 μm and 12.5 μm are similar (∼22″) (see Fig. 1). The latter is dominated by the [NeII] 12.8 μm line as derived from the ISO SWS spectrum (Peeters et al. 2002) and the former is dominated by Brγ emission as seen in Fig. 3. The Brγ image displays a morphology very similar to the radio continuum map, with a cometary shape, and a peak which is essentially coincident with the radio continuum one. Due to the interferometric nature of the radio continuum observations, the sensitivity to extended structures is a function of both the details of the source structure and the (u,v) coverage during observations. For this reason it is a dangerous (and probably unreliable) exercise to derive an extinction map based on the ratio between the Brγ and radio continuum images. The similar morphology between the two maps suggests that there are no steep extinction gradients across the region, and, most probably, the UCHII region is on the observer's side of the molecular cloud.

Several near-IR sources are found immersed in this nebulosity. Two sources with near-IR excess, reported in Table 1 (#13 and #15), are very close to the radio peak (see Fig. 9) while 14 other IR-excess objects are located within the boundaries of the nebulosity (see Fig. 9). With one exception, all these sources occupy a well-defined region in the K vs. $H-K$ diagram (Fig. 6), suggesting spectral types in the range B0–B8 and extinctions in the range $A_V=13-25$, depending on the strength of their infrared excess. One source, located at $\alpha_{2000}=18^{\rm h}06^{\rm m}13.96^{\rm s}$; $\delta_{2000}=-20^\circ31'44.6''$, less than 2″ away from the mid-IR peak as measured by MSX is the reddest and brightest ($K=13.69$, $H-K=3.25$ and undetected at J) in the vicinity. The colors and IR luminosity indicate that it is an O-type star more deeply embedded in the cloud ($A_V>25$). This young stellar object appears point-like on our images and most probably is the single most important contributor of ionizing energy to G9.62+0.19 B as it alone can account for the required UV photons.

Thus, the presence of an embedded young stellar cluster in G9.62+0.19 B is established. As is common in these recently born massive clusters, the most massive O-type star is located near its center and is surrounded by more than a dozen less massive stars of spectral types earlier than B2-B3, most of them showing significant IR-excess. This implies a very short age.

3.2.2. G9.62+0.19 C

A very red nebulosity is associated with this radio UC HII region which appears cometary with a size of about 4–5″ (Garay et al. 1993, see Figs. 2 and 3).

In contrast to component B discussed above, our Brγ map only shows a faint nebular emission coincident with the tail of the cometary UCHII region. This suggest that a strong

Table 1. Position and photometry of the sources in G9.62+0.19 with near-IR excess.

Source	α(2000)	δ(2000)	J	H	K
	h m s	° ′ ″	mag	mag	mag
1	18 06 11.61	–20 31 59.5	18.60(.12)	17.25(.12)	15.20(.06)
2	18 06 12.12	–20 31 21.2	18.67(.20)	16.46(.12)	13.90
3	18 06 12.15	–20 32 12.0	19.11(.20)	15.07(.06)	12.00
4	18 06 12.33	–20 31 49.7	17.77(.07)	18.00(.21)	15.43(.07)
5	18 06 12.84	–20 31 12.1	17.98(.09)	17.29(.25)	14.14
6	18 06 12.92	–20 32 11.2	17.53(.08)	14.20(.11)	11.82
7	18 06 12.99	–20 31 12.3	19.25(.13)	18.92(.19)	16.08(.16)
8	18 06 13.19	–20 31 49.8	19.46(.26)	17.84(.09)	14.60
9	18 06 13.38	–20 32 04.2	13.82	12.44	10.84
10	18 0613.50	–20 31 40.6	19.03(.22)	17.95(.19)	16.18(.16)
11	18 06 13.59	–20 31 33.9	18.70(.17)	17.66(.14)	15.95(.12)
12	18 06 13.99	–20 31 33.3	18.49(.12)	17.42(.20)	15.65(.09)
13	18 06 14.03	–20 31 41.3	18.22(.14)	16.83(.10)	15.06(.14)
14	18 06 14.07	–20 31 35.4	18.54(.13)	17.41(.09)	15.54(.14)
15	18 06 14.08	–20 31 42.4	18.75(.15)	17.59(.11)	15.16(.15)
16	18 06 14.13	–20 31 32.3	18.71(.16)	16.89(.08)	15.07(.09)
17	18 06 14.15	–20 31 25.2	19.59(.14)	17.82(.16)	14.41(.13)
18	18 06 14.21	–20 31 20.9	19.35(.14)	16.97(.07)	14.83(.17)
19	18 06 14.33	–20 31 50.1	18.92(.21)	17.80(.14)	15.55(.15)
20	18 06 14.34	–20 31 54.1	19.61(.32)	18.48(.20)	16.65(.12)
21	18 06 14.40	–20 32 08.9	19.09(.18)	15.44(.09)	11.50
22	18 06 14.48	–20 31 48.6	17.59(.07)	16.23	14.72(.10)
23	18 06 14.59	–20 31 53.4	19.35(.24)	18.62(.24)	16.12(.16)
24	18 06 14.59	–20 31 48.4	19.46(.31)	17.51(.13)	15.17(.14)
25	18 06 15.31	–20 31 27.2	18.57(.11)	17.33(.11)	15.79(.18)
26	18 06 15.62	–20 32 07.5	19.32(.26)	17.20(.12)	14.78
27	18 06 16.92	–20 31 22.5	19.09(.16)	18.77(.17)	17.00(.16)

extinction gradient is present in the region, and that the head of the cometary UCHII region is still embedded within the molecular cloud. Given also the lack of molecular hydrogen emission (Fig. 2), the nebular emission detected in the near infrared broad-band filters is most probably due to very red continuum emission, possibly due to the cloud material heated by the cluster of bright massive YSOs (see below).

Eight near-IR sources in our survey appear to be immersed in a diffuse near-IR nebulosity as shown in Fig. 10. At its eastern edge lies the peak emission of the radio component C. The list of these sources with their position and photometry is given in Table 2.

Three point-like near-IR objects lie to the NW, outside of the lowest 3.6 cm emission mapped by the VLA (Testi et al. 2000), though they are probably immersed in the *extended* lower brightness continuum emission, thus undetected by the VLA around the UC HII region (cf. Kurtz & Franco 2002). The brightest of them (at K), source c1, shows marginal or no 2.2 μm excess emission and occupies the locus of an O6-7 star obscured by $A_V \simeq 15{-}25$ in the $H-K$ vs. $J-H$ and K vs. $H-K$ diagrams. Although this object is located some 10″ (0.27 pc) away from the peak radio-continuum emission, this star probably plays an important role in the ionization of the gas.

Two other sources, c3, c4, show JHK colors revealing significant near-IR excesses. From their position in the K vs. $H-K$ plot and allowing for their K-band excess emission, their spectral types range from O9 to B3 and $A_V \simeq 20{-}25$. Sources c5, c6, c7 are too faint at J to be detected. From their HK magnitudes, we infer that they also are massive O-type very young stars reddened by more than $A_V = 25$. Source c7 deserves

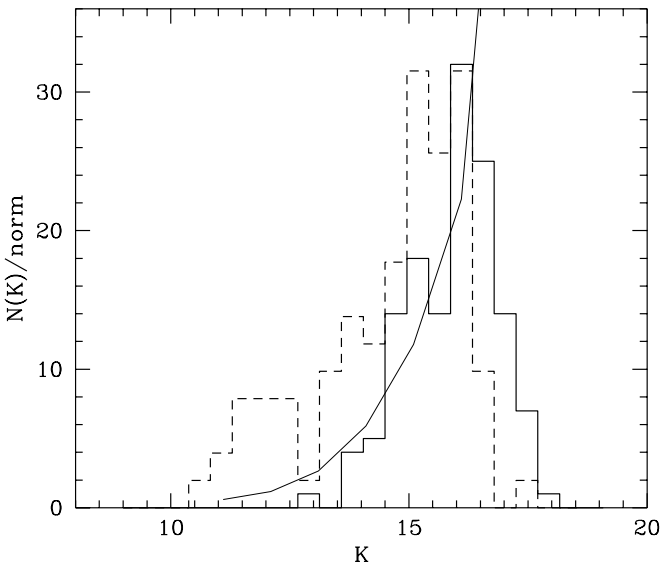

Fig. 8. Comparison of the K-magnitude distribution of the IR-excess sources identified as young stars including those with $H-K > 2$ (dashed line), of stars without significant IR-excess (thick continuous line) and of field stars in a neighboring region (thin continuous line). See Sect. 3.1.

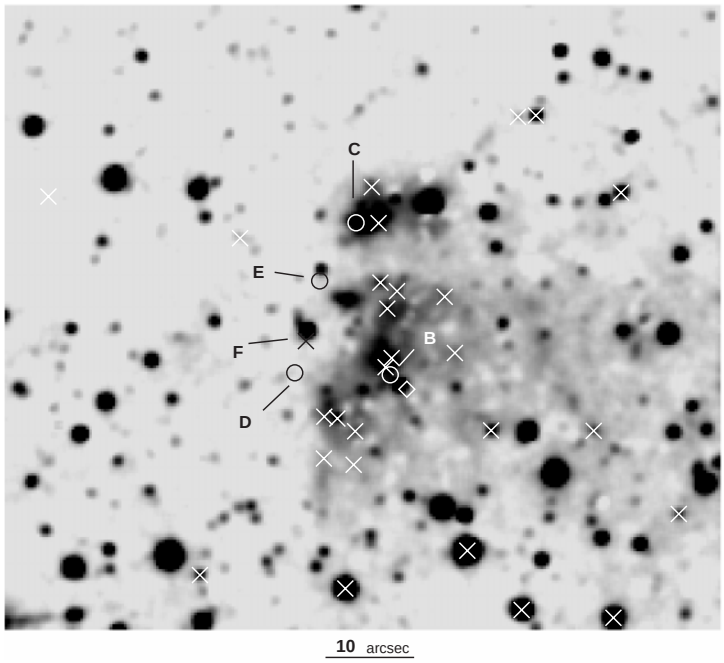

Fig. 9. K-band image of the central region of G9.62+0.19 ($89'' \times 89''$), indicating the position of the UC HII regions (open circles), the hot core (black cross) and of the sources with IR excesses (white cross). The diamond indicate the peak position of the extended mid-IR source. North is to the top, east to the left.

particular attention. It is the reddest ($H - K = 4.9 \pm 0.40$) member of this compact cluster. It is located within $1''$ of the radio peak and almost at the geometrical center of the UC HII region. It occupies an extreme position on the K vs. $H - K$ diagram revealing a high luminosity and strong excess emission at $\lambda > 2\,\mu$m, apart from large obscuration ($A_V > 28$), similar to IR source associated with component F, the densest hot molecular core (see sect. 3.3.4). The fainter source c8 is even closer to the radio peak but is too faint to be detected even at H. None of these sources was bright enough at 12.5 μm to appear above the noise on our mid-IR image.

3.3. Radio components inside the dense core

3.3.1. G9.62+0.19 D

This is smaller cometary UC HII region with an angular size of $\leq 2''$ and excited by a B0.5 ZAMS star (Hofner et al. 1996; Testi et al. 2000). H_20, OH and CH_3OH masers are found in this region (Hofner & Churchwell 1996; Forster & Caswell 1989; Norris et al. 1993). We detected a faint source with $K = 16.44 \pm 0.12$ at a distance $+1.5''$ in RA and $+0.7''$ in Dec from the radio peak. At present, we cannot confirm the identification of the near-IR sources with the UC HII.

3.3.2. G9.62+0.19 E

Component E is located at the edge of the molecular cloud core observed in $C^{18}O$. It has been interpreted by Hofner et al. (1996) to be a young massive star surrounded by a very small UC HII region (recently classified as hyper-compact HII region by Kurtz & Franco 2002) within a dusty envelope. OH and

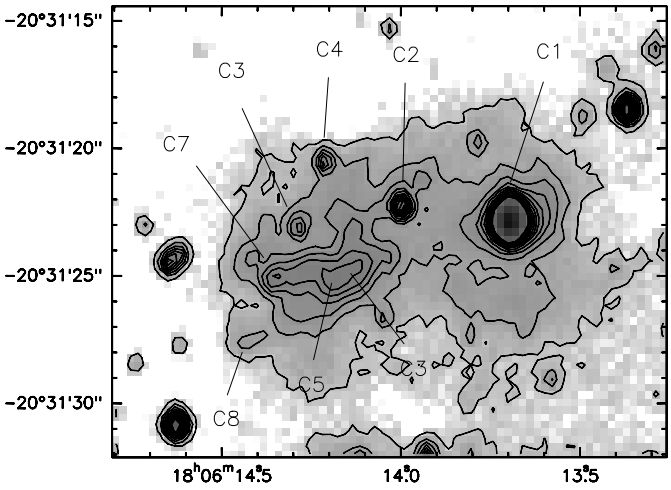

Fig. 10. SofI K_s image of the UC HII region C with the identifications of the near-IR sources. The coordinates are the epoch 2000.

H_2O masers have also been reported in the vicinity (Forster & Caswell 1999). No near or mid-infrared source has been found associated with UC HII E. A star without near-IR excess is located approximately $1.4''$ N of the radio peak and its JHK colors suggest that it may be field star; this NIR source was associated to the radio component by Testi et al. (1998), however, our higher angular resolution observations and improved astrometric accuracy, suggest that the two sources are not physically related.

Table 2. Positions and photometry of the sources associated with the UC HII region G9.62+0.19 C.

Source	α(2000)	δ(2000)	J	H	K	Remarks
	h m s	° ′ ″	mag	mag	mag	
c1	18 06 13.72	–20 31 22.8	15.89	13.38	11.57	no IR excess
c2	18 06 14.01	–20 31 22.5	18.36(.08)	16.23	14.71(.11)	no IR excess
c3	18 06 14.15	–20 31 25.2	19.59(.14)	17.82(.16)	14.41(.13)	neb.
c4	18 06 14.22	–20 31 20.6	19.35(.14)	16.97(.07)	14.83(.17)	
c5	18 06 14.24	–20 31 24.8		17.51(.11)	14.41(.13)	neb.
c6	18 06 14.29	–20 31 23.1		18.67(.22)	14.81(.14)	
c7	18 06 14.34	–20 31 25.0		19.27(.38)	14.29(.13)	UC HII-C
c8	18 06 14.42	–20 31 27.4			15.57(.13)	

3.3.3. G9.62+0.19 G, H, I

Testi et al. (2000) found within the dense core of G9.62+0.19 three new weak radio sources detected at 2 and 3.6 cm named G, H and I. Very close to the radio peaks H and G, we detected two near-IR sources at: $\alpha_{2000} = 18^{\rm h}06^{\rm m}15.04^{\rm s}$; $\delta_{2000} = 20°31'35.7''$ ($K = 15.74$, $J - H = 1.36$, $H - K = 1.26$) and $\alpha_{2000} = 18^{\rm h}06^{\rm m}14.81^{\rm s}$; $\delta_{2000} = 20°31'37.0''$ ($K = 15.24 \pm 0.14$, $J - H = 1.44$, $H - K = 0.84$), respectively. Most probably these are not associated to the star forming region, as their observed JHK colors imply that these are field stars. No IR emission has been detected towards component I.

3.3.4. G9.62+0.19 F (Hot Molecular Core, HMC)

This small hot and dense molecular clump detected through the thermal line emission of CH_3OH and NH_3 and also in the 7 mm thermal continuum (Cesaroni et al. 1994; Hofner et al. 1994, 1996), is also the site of several molecular masers. It is the site of recent formation of a massive (system of) massive star(s), which is believed to be at a very early stage of its life. Testi et al. (2000) detected a compact faint centimeter radio continuum source near the center of the HMC. Its radio emission is consistent with thermal emission from ionized gas, coming from a strong ionized stellar wind or from a *hyper-compact* HII region. Surprisingly (because of the extremely high obscuration expected) a near-IR source had been found at this position by Testi et al. (1998). Interestingly enough, Hofner et al. (2001) reported the detection of a CH_3OH high-velocity bipolar outflow centered very close to the radio and near-IR source. This outflow is apparently seen almost pole-on, which would explain the lower-than-expected line-of-sight obscuration towards the central star as the dust has been partially cleared by the escaping material (Hofner et al. 2001).

The present higher resolution near-IR observations confirm the existence of such an object, with a very red color ($K = 13.41$ and $H - K = 5.2 \pm 0.2$ and fainter in J than our detection limit). Its location in the K vs. $H - K$ diagram is extreme: it is the object with the largest $H - K$ color index in our sample, implying a very large K-band excess and obscuration $A_V > 28$ as well as a high luminosity.

This source was also detected on our 12.5 μm image (see Fig. 2). Its measured position is $\alpha_{2000} = 18^{\rm h}06^{\rm m}14.7^{\rm s}$; $\delta_{2000} = -20°31'38''$, less than $2''$ to the NW of the nominal position of the HMC. We believe that this is the same point-like source observed at 10 and 18 μm by De Buizer et al. (2000) and which, lacking a good astrometric reference, they identified with component D. Their reported 10 and 18 μm fluxes are totally consistent with the 12.5 μm flux reported in this work.

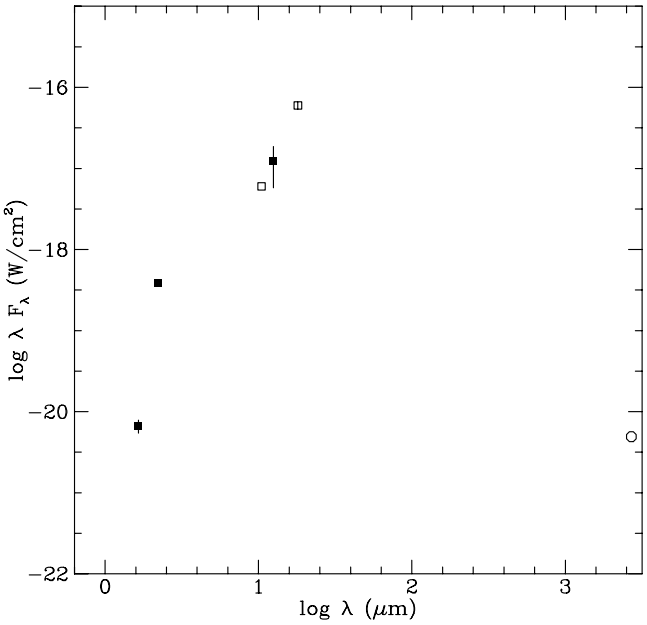

Fig. 11. Spectral energy distribution of the component F. Data sources are: filled squares from this work, open squares from De Buizer et al. (2000), and circle from Hofner et al. (1996).

Combining the near and mid-IR observations, we derived the spectral energy distribution (SED) presented in Fig. 11. The short wavelength flux rises very steeply with the K flux density probably enhanced. This could be caused by line circumstellar emission in the K band. This may be the central source of the molecular outflow seen pole-on, although its integrated infrared luminosity is $\sim 10^3\ L_\odot$ (for $d = 5.7$ kpc), well below that required to provide the mechanical energy to drive the molecular flow (Hofner et al. 2001) but close to that needed to explain the observed thermal radio continuum (Testi et al. 2000). It is also possible that more than one YSOs is embedded in the HMC, which would explain why the mid-IR and the ammonia emission seem to arise from slightly different positions.

Finally, a very peculiar extended and double-peaked bright K-band source is located at $\alpha_{2000} = 18^{\rm h}06^{\rm m}14.4^{\rm s}$; $\delta_{2000} = -20°31'34''$. Its shape is elongated ($\sim 3''$) in the E-W

direction and the integrated flux at 2.2 μm is 2 mJy and undetected at H (< 0.06 mJy). This source is the only one detected on our H_2 image shown in Fig. 2, while absent in Brγ, implying shocked gas emission. Naturally, this nebulous object is interpreted as a reddened Herbig-Haro object associated with the high-velocity molecular outflow. Consistent with this interpretation, the HCO^+ map by Hofner et al. (2001) shows at this position an elongation of the blue-shifted emission.

4. Conclusions

We have imaged at high sensitivity and sub-arcsec resolution in the near-and mid-IR the complex star forming region G9.62+0.19. From the analysis of these images we reached the following conclusions:

1) In an area of size 89″×89″ centered on the so-called Hot Molecular Cloud (HMC), approximately 33% of the 292 sources detected on the K images, showed near-IR excesses (Fig. 5) or $H-K \geq 2.0$ (Fig. 6). These have been identified as young stellar objects belonging to the star-formation region. Most of these sources are located outside the dense core observed in $C^{18}O$ by Hofner et al. (1996) and lie within the boundaries of the radio HII region B (Fig. 7). Analysis of the color-magnitude diagram (Fig. 6), and the K-magnitude distribution (Fig. 8) indicate that the young stellar population is dominated by B2-B3 stars reddened by $A_V = 18-25$.

2) Another small cluster of at least 8 young embedded ($A_V \sim 25$) stars is associated with the UC HII region C (Fig. 10) located outside and to the north of the dense core. In particular, the radio peak is coincident with a very red source ($H-K = 4.9$) immersed in a diffuse nebulosity observed at 2.2 μm. From their position in the K vs. $H-K$ diagram, we found that the most luminous sources appear be O-type stars.

3) A more dispersed cluster of bright IR-excess is located to the south of the main complex. These appear to be OB stars less obscured than most of the stars in the embedded clusters.

4) Two sources were detected at 12.5 μm. One is extended and coincides with the HII region B. The second is a fainter, point-like, object within the dense molecular core F (Figs. 1 and 4) which is also detected in the near-IR. It shows a steep infrared energy distribution (Fig. 11), with $H-K = 5.2$. The derived IR luminosity indicates the presence of a very young embedded star of spectral type B3.

At present, it is uncertain what is the required luminosity of the energy source to drive the high-velocity molecular outflow associated with the HMC (Hofner et al. 2001). Thus, we cannot be certain that this unresolved infrared source is indeed the energy provider for the flow.

5) In the other two UC HII regions in the dense core, components D and E, no infrared sources have been found associated with the radio peaks.

The several components of the G9.62+0.19 complex appear to be at different evolutionary stages of their early evolution and the present infrared observations support this view.

Acknowledgements. Part of this work was supported by a CNR (Italy)-Conacyt (Mexico) bilateral agreement. MT also acknowledges grants from Conacyt and DGAPA-UNAM (IN-105400).

References

Alard, C. 2000, A&AS, 144, 363
Cesaroni, R., Churchwell, E., Hofner, P., Walmsley, C. M., & Kurtz, S. 1994, A&A, 288, 903
De Buizer, J. M., Piña, R. K., & Telesco, C. M. 2000, ApJS, 130, 437
Egan, M. P., Price, S. D., Moshir, M. M., et al. 1999, Air force Research Lab. Tech. Rep. no. AFRL-VS. T. R. 1999-1522
Epchtein, N., Deul, E., Derriere, S., et al. 1999, A&A, 349, 236
Forster, J. R., & Caswell, J. L. 1989, A&A, 213, 339
Forster, J. R., & Caswell, J. L. 1999, A&AS, 137, 43
Garay, G., Rodriguez, L. F., Moran, J. M., & Churchwell, E. 1993, ApJ, 418, 368
Hofner, P., & Churchwell, E. 1996, A&AS, 120, 283
Hofner, P., Kurtz, S., Churchwell, E., Walmsley, C. M., & Cesaroni, R. 1994, ApJ, 429, L85
Hofner, P., Kurtz, S., Churchwell, E., Walmsley, C. M., & Cesaroni, R. 1996, ApJ, 460, 359
Hofner, P., Wiesemeyer, H., & Henning, Th. 2001, ApJ, 549, 425
Koornneef, J. 1983, A&A, 128, 84
Kurtz, S., & Franco, J. 2002, Rev. Mex. Astr. Astrofis. Conf. Ser., 12, 16
Kurtz, S., Churchwell, E., & Wood, D. O. S. 1994, ApJS, 91, 659
Norris, R. P., Whiteoak, J. B., Caswell, J. L., Wieringa, M. H., & Gough, R. G. 1993, ApJ, 412, 222
Peeters, E., Martín-Hernández, N. L., Damour, F., et al. 2002, A&A, 381, 571
Salas, L., et al. 2002, Rev. Mex. Astron. Astrofis., submitted
Stetson, P. B. 1987, PASP, 99, 191
Testi, L., Felli, M., Persi, P., & Roth, M. 1998, A&A, 329, 233
Testi, L., Hofner, P., Kurtz, S., & Rupen, M. 2000, A&A, 359, L5